One-step synthesis of <001>-oriented PbTiO$_3$ nanoplates for templated grain growth by a hydrothermal method

Xing-Hua Ma[1,*] ⓘ, Junjia Xia[1], and Shuling Zhang[1]

[1] School of Mechanical & Automotive Engineering, Qingdao University of Technology, Qingdao 266520, Shandong, China

ABSTRACT

<001>-oriented PbTiO$_3$ nanoplates with an average aspect ratio of approximately 5 were synthesized by a one-step hydrothermal method. The factors that could affect the growth of the PbTiO$_3$ nanoplates, such as the concentration of the mineralizer (KOH) and ratio of Pb^{2+}/Ti^{4+} in the source materials, were carefully investigated. A modified growth process of the PbTiO$_3$ nanoplates was proposed by a time variation evaluation. Therefore, the typical growth parameters were set to 200 °C/10 h, Pb^{2+}/Ti^{4+} = 1.25 (M$_{p25}$ = 5 mmol and M$_{Pb(NO3)2}$ = 6.25 mmol), and M$_{KOH}$ = 8 mol/L (in 30 ml of DI water) with P25-TiO$_2$ and Pb(NO$_3$)$_2$ as the source materials. Furthermore, the d_{33} versus applied voltage curve showed good ferroelectric behavior with a maximum d_{33} value of ∼ 165 pm/V, indicating promising potential as seeds for templated grain growth (TGG) of PbTiO$_3$ nanoplates.

1 Introduction

To develop high-performance electroceramics, many investigations have been performed, such as phase boundary engineering by composition design [1–4], element or compound additive doping [5–8], and the preparation of textured ceramics [9, 10]. Among these studies, the textured piezoelectric ceramics produced by the templated grain growth (TGG) process have received considerable attention since the corresponding properties of the as-made ceramics could be comparable to those of their single crystal forms [11, 12]. During the TGG process, a small percentage of oriented-plates with single crystallinity are mixed with the matrix powders and then oriented-processed by a shear process (tape casting or extrusion, etc.). Subsequently, with continued heat treatment, the volume of the oriented parts will increase with the growth of the larger, oriented grains by consuming the matrix based on the template plates, resulting in highly textured ceramics. Because of the existence of a high degree of texture in the polar direction, the textured ceramics could exhibit a fair number of properties of single crystal forms [12, 13].

To successfully produce textured ceramics, the template crystals should meet several requirements. First, the templates should have high aspect ratios

with proper sizes and suitable crystallographic orientation. More importantly, the lattice parameter mismatch between the template crystal and the matrix crystal should be lower than 15% so that the matrix phase can nucleate and grow from the oriented templates at the specific heat treatment temperature [14].

So far, $SrTiO_3$, $BaTiO_3$ and $Bi_4Ti_3O_{12}$, etc. have usually been used as templates for the TGG process to obtain textured piezoelectric ceramics [15–18], but the disadvantages of these templates cannot be ignored. For example, a two-step chemical conversion process (a precursor with plate-like morphology is synthesized first by molten salt synthesis with NaCl and/or KCl working as the salts, and then the as-synthesized precursors are converted into the final perovskite plates through a topochemical reaction) is usually employed to synthesize the plates. For example, $BaTiO_3$ and $SrTiO_3$ have been reported to convert from plate-like $BaBi_4Ti_4O_{15}$ and $Sr_3Ti_2O_7$, respectively [19, 20]. However, such a process is complex and time consuming. Furthermore, extremely high temperature (over 1000 °C) heat treatments are always employed [19, 20].

Though the research on lead-free piezoelectric ceramics has received more and more attention, Pb-based (especially $PbTiO_3$- or $Pb(Zr, Ti)O_3$-based) ceramics are still the major choice for real applications due to their much superior and more stable properties than that of lead-free ceramics [21–24]. Therefore, to make textured lead-based ceramics, $PbTiO_3$ nanoplates could be good candidates for the TGG process because of their much smaller lattice mismatch with $PbTiO_3$ (or $Pb(Zr, Ti)O_3$)-based matrix ceramics. To date, several studies have reported the synthesis of $PbTiO_3$ nanoplates [25, 26]. For example, Chao et al. employed $Pb(NO_3)_2$ and TiO_2 powders as source materials to synthesize $PbTiO_3$ nanoplates via a hydrothermal process [25]. For this research, there are still some interesting and valuable results worth further clarifying. For example, we have investigated the effect of different TiO_2 sources on the final morphology of $PbTiO_3$ products and found that $P25-TiO_2$ (a kind of special TiO_2 powder composed of anatase and rutile crystallites [27]) was the best TiO_2 source material to synthesize uniform $PbTiO_3$ nanoplates due to the hydrophilicity and fine particle size of the $P25-TiO_2$ powder [28]. In addition to the categories of source materials, the ratio among the reactants could also greatly affect the

final products [29, 30]. Therefore, it is worth studying the effect of Pb^{2+}/Ti^{4+} ratio in the source materials on the shape and composition of the $PbTiO_3$ nanoplates, and a modified growth process of the $PbTiO_3$ nanoplates was further explored in the current work. Additionally, in the hydrothermal synthesis process, a mineralizer is generally used to control the morphology of the products since it is conducive to crystallization [31]. Perovskite crystals tend to be formed in an alkaline environment, so KOH is normally used as the mineralizer [32–34]. Although the effect of KOH was also reported in Chao's paper, the exact amount of KOH was not clear [25]. Thus, it is necessary to briefly describe the effect of KOH concentration. Furthermore, the piezoelectric coefficient (d_{33}) was measured using contact mode piezoelectric force microscopy (PFM) to study the ferroelectricity of the $PbTiO_3$ nanoplates and their potential as seeds for templated grain growth.

2 Experimental Procedures

$PbTiO_3$ nanoplates were synthesized with high purity chemicals (> 99%) by the hydrothermal method. Lead (II) nitrate ($Pb(NO_3)_2$, 99.99%, High Purity Chemicals, Osaka, Japan) and $P25-TiO_2$ (> 99%, Evonik Corporation, Parsippany, USA) were used as the source materials. Analytical grade solid potassium hydroxide (KOH, > 99%, High Purity Chemicals, Osaka, Japan) acted as the mineralizer. For the specific synthesis processes, $P25-TiO_2$ powders were first added into 30 ml of DI water mixed with 8 mol/L KOH to form a milky white suspension. Then, 10 ml of $Pb(NO_3)_2$ solution was injected into the suspension dropwise. Here, to clearly clarify the effect of the Pb/Ti ratio, two different conditions regarding the amount of the starting Ti and Pb sources were set: (i) $P25-TiO_2$ is 5 mmol with different amounts of $Pb(NO_3)_2$ and (ii) $Pb(NO_3)_2$ is 6.25 mmol with different amounts of $P25-TiO_2$. The stirring rate was kept at 600 rpm throughout the whole process.

After thoroughly mixing by magnetic stirring for approximately 2 h, the solution gradually transformed into a red color (this phenomenon of the color change will be explained in the latter part). Then it was transferred into a stainless-steel autoclave, heated directly in an oven at 200 °C for 10 h and cooled to room temperature in air. The resulting

samples were filtered and washed with deionized water and ethanol several times and dried for the following characterizations.

The phase structure of the specimens was identified by X-ray diffraction (XRD; Rigaku D/max-RC, Tokyo, Japan) with Cu Kα radiation ($\lambda = 1.5418$ Å). Microstructural observation was performed using scanning electron microscopy (SEM; Hitachi S-4300, Tokyo, Japan). The mean lateral size and thickness of the nanoplates were analyzed from the digitized images with Image Tool software [35]. High-resolution transmission electron microscopy (HRTEM; Tecnai F20, FEI, the Netherlands) was carried out to analyze the oriented direction of the exposed crystal plane of the as-synthesized nanoplates. Piezoelectric force microscopy (Dimension 3100, Veeco Instruments, Plainview, NY) and a lock-in amplifier (SR830, Stanford Research Systems) were employed to measure the d_{33} value of the PbTiO$_3$ nanoplates.

3 Results and discussion

After the reaction and following treatment (cleaning and drying), the product powders show a yellow color, indicating the successful growth of the PbTiO$_3$ nanoplates. Typical TEM images of the as-synthesized PbTiO$_3$ nanoplates are shown in Fig. 1. Figure 1a shows a low-resolution TEM image of a PbTiO$_3$ nanoplate with a square morphology. The corresponding high-resolution TEM (HRTEM) image is shown in Fig. 1b, and well-ordered lattice fringes and the corresponding fast Fourier transform pattern (FFT, inset of Fig. 1b) could be obtained. Both lattice distances along the two directions are determined to be ~ 0.39 nm and the intersection angle between them is $\sim 90°$, which matches well with the (100) and (010) planes of the tetragonal PbTiO$_3$ crystal structure. Furthermore, the spot pattern of the FFT is proven to be the {$hk0$} set reflections. Therefore, these analyses confirm that the PbTiO$_3$ nanoplates are bounded by the {100} planes and oriented with an exposed plane of {001} of the perovskite tetragonal structure [25, 28]. The effect of KOH concentration on the growth of PbTiO$_3$ nanoplates was also studied and the corresponding results are shown in Fig. S1 (Supplementary Material). Based on the analysis, the optimum concentration of KOH in the starting materials should be approximately 8 mol/L in 30 ml of DI water since the morphology of the nanoplates

was more uniform. In addition to KOH, NaOH or NH$_3$·H$_2$O has also been used as a mineralizer [36, 37], and their effect on the growth of PbTiO$_3$ nanoplates is still under way.

3.1 The effect of Pb^{2+}/Ti^{4+} ratio

In addition to the effect of source materials and the concentration of the mineralizer, the molar ratio between Pb^{2+} and Ti^{4+} in the starting materials also strongly affects the formation of the PbTiO$_3$ products in the hydrothermal synthesis process, as demonstrated by the model proposed by Lencka et al. [38]. Different from the former report, here, we discussed this effect in two ways according to the initial amount of Pb^{2+} and Ti^{4+}: (i) Pb^{2+}/Ti^{4+} = 1 – 2.5 with M$_{P25}$ = 5 mmol; (ii) Pb^{2+}/Ti^{4+} = 1.25 – 2.5 with M$_{Pb(NO3)2}$ = 6.25 mmol.

The SEM images of the final products with the Pb^{2+}/Ti^{4+} ratio from 1 to 2 in the source materials (Condition (i)) are shown in Fig. 2. When the ratio of Pb^{2+}/Ti^{4+} was 1, the products were mainly composed of cracked nanoplates and irregular crystals (Fig. 2a). This should be due to the less amount of backbones, i.e., there were not enough PbO crystals to react with P25-TiO$_2$ nanoparticles to form regular PbTiO$_3$ nanoplates (the role of PbO crystals will be explained in detail in Part 3.2 and Fig. S2 of the Supplementary Material). When Pb^{2+}/Ti^{4+} reached 1.25 to 1.5, the backbones supplied by the PbO crystals for the resulting nanoplates were enough for the latter reaction with P25-TiO$_2$ powder, leading to well-formed PbTiO$_3$ nanoplates with a lateral size of ~ 1 μm and thickness of ~ 200 nm as shown in Figs. 2b and c. However, if the amount of Pb^{2+}/Ti^{4+} was further increased to 2, aggregation occurred, as shown in Fig. 2d, due to the excessive PbO crystals. The SEM image of the specimen with Pb^{2+}/Ti^{4+} of 2.5 is not shown here due to its similar morphology with that of Fig. 2d. The corresponding XRD patterns of the products with the Pb^{2+}/Ti^{4+} ratio from 1.25 to 2 are shown in Fig. 3a–c, respectively. All the products show a pure perovskite phase without any other secondary phases. Furthermore, compared with the standard JCPDS card (# 70–0746), the relative intensity of (001)/(100) is greatly enhanced for Fig. 3a and b, indicating that the preferential growth planes of the PbTiO$_3$ nanoplates are the {001} crystal planes. This could also be proven by TEM analysis, which is shown in Fig. 1. However, when the ratio of Pb^{2+}/

Fig. 1 **a** Low magnification and **b** high resolution TEM images of the as-synthesized $PbTiO_3$ nanoplates. The inset image of **b** shows the corresponding fast Fourier transform (FFT) pattern of the nanoplate
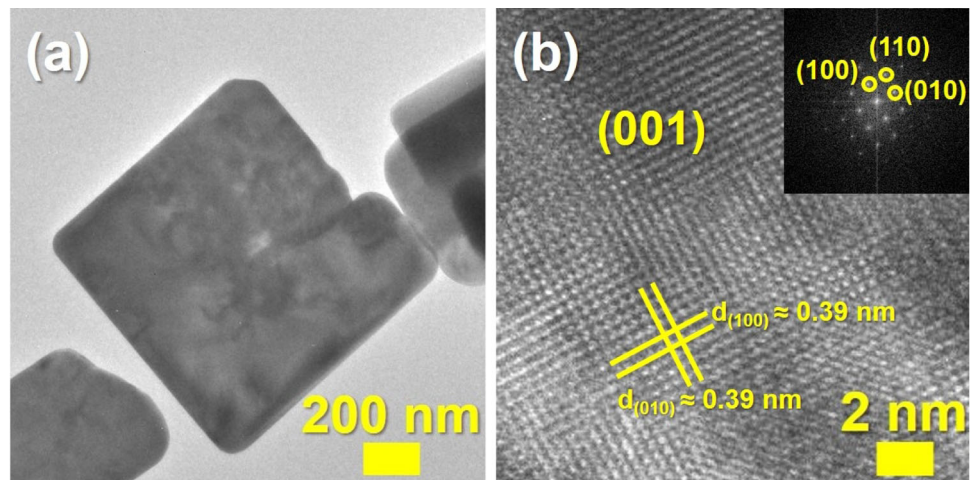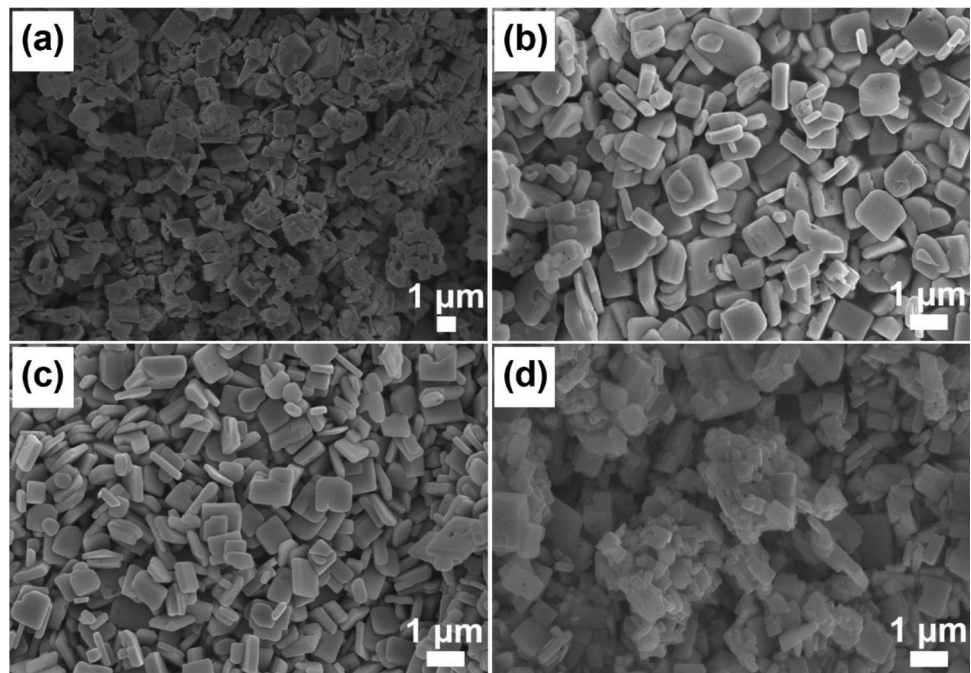

Fig. 2 SEM images of the $PbTiO_3$ nanoplates produced with Pb^{2+}/Ti^{4+} molar ratios of **a** 1, **b** 1.25, **c** 1.5 and **d** 2 with an initial $M_{P25} = 5$ mmol

Ti^{4+} reached 2.5, Pb^{2+} was so excessive (approximately 4.14 g in the source materials) that the PbO phase was found in the final products, as indicated by XRD (Fig. 3d). Thus, for this condition, the appropriate ratio of Pb^{2+}/Ti^{4+} is 1.25 to 1.5.

For Condition (ii), Fig. 4a–c show the SEM images with Pb^{2+}/Ti^{4+} equal to 1.5, 2 and 2.5, respectively. The corresponding XRD patterns are shown in Fig. 3e–g. Different from the phenomenon observed in Condition (i), when the Pb^{2+}/Ti^{4+} ratio reached 2.5, no secondary phase could be detected by XRD (Fig. 3g). This difference might be due to the relatively low amount of $Pb(NO_3)_2$ compared with that of

Condition (i). Although slight aggregation could also be found (Fig. 4c), the relative intensity of the (001)/ (100) peak was still greatly enhanced for the ratio of 2.5. Therefore, for Condition (ii), the appropriate ratio of Pb^{2+}/Ti^{4+} could be 1.25 to 2.5. However, based on the results of the above two cases, the best ratio of Pb^{2+}/Ti^{4+} should be 1.25 since it has the highest (001)/(100) relative peak intensity, which could reveal the preferential growth planes of the $PbTiO_3$ nanoplates.
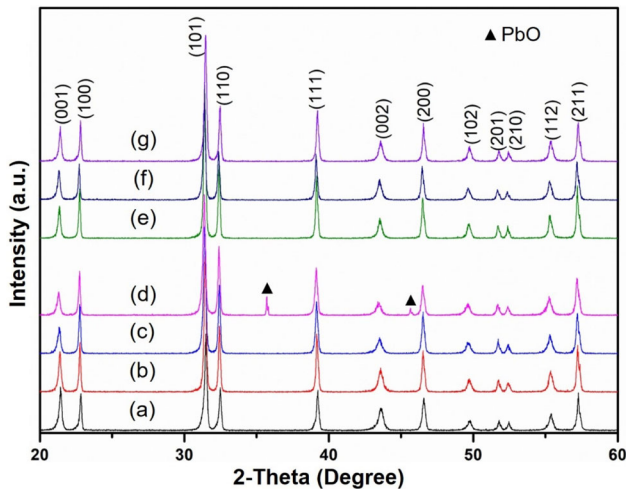
Fig. 3 XRD patterns of the PbTiO$_3$ nanoplates produced with Pb^{2+}/Ti^{4+} molar ratios of **a** 1.25, **b** 1.5, **c** 2, and **d** 2.5 with an initial M$_{P25}$ = 5 mmol and **e** 1.5, **f** 2, and **g** 2.5 with an initial M$_{Pb(NO3)2}$ = 6.25 mmol

3.2 The effect of heating time and the corresponding growth process

Last but most importantly, experiments according to time variations were performed to explore the detailed growth process of the PbTiO$_3$ nanoplates. Figure 5a shows the SEM image of the initial mixture of the source materials (i.e., the specimen without hydrothermal treatment). As indicated by the SEM image at low magnification, the products were composed of bulk crystals and tiny lamellate particles; however, from the observation at a higher magnification (inset of Fig. 5(a)), these bulk crystals were actually several thinner nanoplates stacked layer by layer. The tiny lamellate particles should come from the P25-TiO$_2$ source powder, which was observed in our previous research [28]. Therefore, these stacked thinner nanoplates might be induced by the Pb source. To evaluate this, only Pb(NO$_3$)$_2$ was added to the alkaline solution without the P25-TiO$_2$ powder. After mixing by magnetic stirring, red-colored crystals precipitated from the transparent solution. This should also be the reason why the milky white suspension transformed into a red color after adding Pb(NO$_3$)$_2$ in the "Experimental Procedures" section. As shown in Fig. S2a (Supplementary Material), the red-colored crystals were recognized to be the PbO phase according to the XRD patterns (JCPDS card #05–0561). The corresponding morphologies were found to be tetragonal-like crystals 5 ∼ 7 μm in
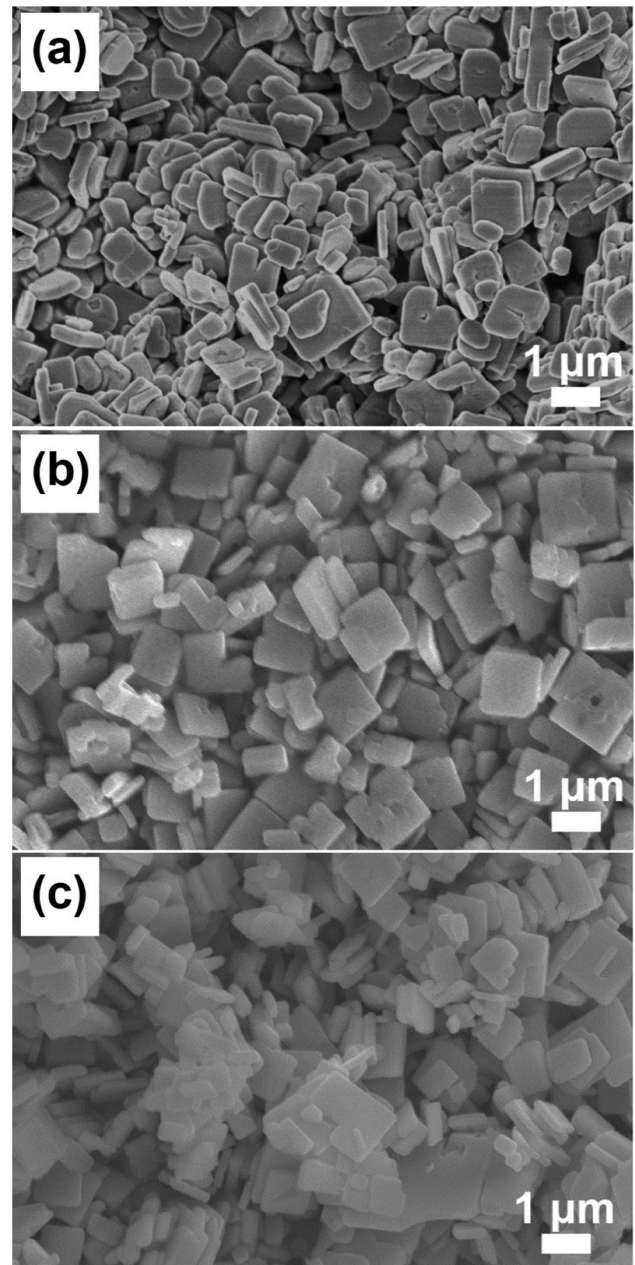

Fig. 4 SEM images of the PbTiO$_3$ nanoplates produced with Pb^{2+}/Ti^{4+} molar ratios of **a** 1.5, **b** 2, and **c** 2.5 with an initial M$_{Pb(NO3)2}$ = 6.25 mmol

size, as shown in Fig. S2b. Furthermore, compared with the standard XRD patterns, the (002) peak intensity was greatly enhanced, indicating that the PbO crystals were oriented with the exposed plane of {001}, which might provide a template for the latter PbTiO$_3$ nanoplate growth. Therefore, it could be concluded that when PbO crystals precipitated from the solution mixed with the P25-TiO$_2$ powder, the larger bulk crystals might be crushed into smaller

Fig. 5 a SEM images of the PbTiO$_3$ nanoplates produced at 200 °C for **a** 0 min, **b** 0.5 h, **c** 5 h, and **d** 10 h; the insets of (**a**) and (**b**) show enlarged SEM images of the parts marked by the circles in (**a**) and (**b**), respectively
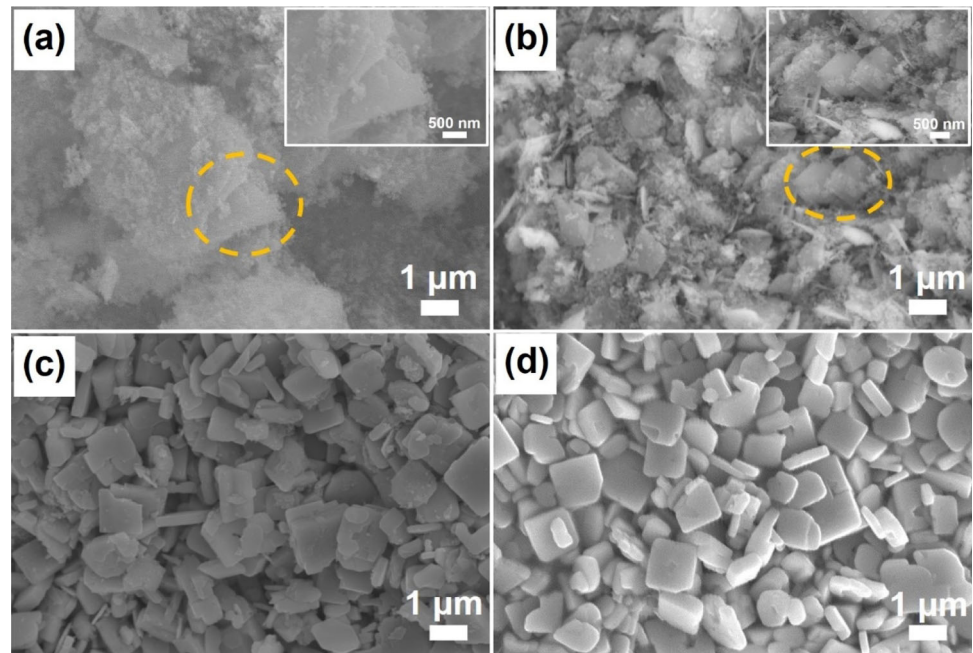
sizes and exfoliated into stacked thinner nanoplates in the alkaline solution by the P25-TiO$_2$ nanoparticles, since without the addition of P25-TiO$_2$ powder, only larger-sized PbO crystals were found in the final products.

Figure 5b shows the SEM image of the specimen synthesized at 200 °C for 0.5 h. The products were still composed of tiny lamellate particles and thin nanoplates (as marked by the circle; inset of Fig. 5b shows the enlarged SEM image of the thin nanoplates). To verify the detailed composition of the mixture, XRD analysis was conducted on the samples synthesized for 0.5 h, which is shown in Figure S3 (Supplementary Material). TiO$_2$, PbTi$_{0.8}$O$_{2.6}$, and PbTiO$_3$ could be indexed in the XRD pattern, which means that the PbO nanoplates reacted with P25-TiO$_2$ nanoparticles to form PbTi$_x$O$_y$ (stoichiometric compound and Pb excess compound, i.e., PbTi$_{0.8}$O$_{2.6}$ and PbTiO$_3$) compounds in a short time. When the reaction time increased to 5 h, thicker nanoplates with rough basal planes appeared and mixed with a small number of nanoparticles, indicating an incomplete reaction (Fig. 5c). Then, the PbTiO$_3$ nanoplates are well formed with a relatively smooth surface as the heating time increases to approximately 10 h, as shown in Fig. 5d.

Based on the above discussion, a possible modified growth process could be proposed as follows, and the corresponding schematic image is shown in Fig. 6.

Before heat treatment, i.e., during the mixing stage, the large PbO crystals were crushed into smaller crystals and exfoliated into stacked nanoplates, as shown in Fig. 6a. This could be proven by the observation in Fig. 5a. Then, in the initial stage of the heat treatment, the exfoliated nanoplates reacted with the surrounding P25-TiO$_2$ nanoparticles to form the PbTiO$_3$ phase and the PbTi$_{0.8}$O$_{2.6}$ phase with nanoplate morphologies in a short time, as proven by the XRD pattern shown in Fig. S3. With increasing heating time, the P25-TiO$_2$ nanoparticles continually reacted with the PbTi$_{0.8}$O$_{2.6}$ phase, and at the same time, the thinner PbTiO$_3$ nanoplates restacked with each other layer by layer along the [001] direction (Fig. 6b). After that, the layered nanoplates transformed into thicker PbTiO$_3$ nanoplates by the so-called surface reconstruction and Ostwald ripening process as proposed by Chao et al. [25] (Fig. 6c).

3.3 The measurement of the d_{33} value

For ferroelectric materials, the piezoelectric coefficient (d_{33}) is one of the most important parameters. To measure the d_{33} value, PbTiO$_3$ nanoplates were first deposited onto Pt/SiO$_2$/Si substrates via the spin coating process, and then piezoelectric force microscopy (PFM) was used to perform the measurement [39].

Figure 7 shows the curve of the d_{33} value versus the applied voltage of the PbTiO$_3$ nanoplates, and the
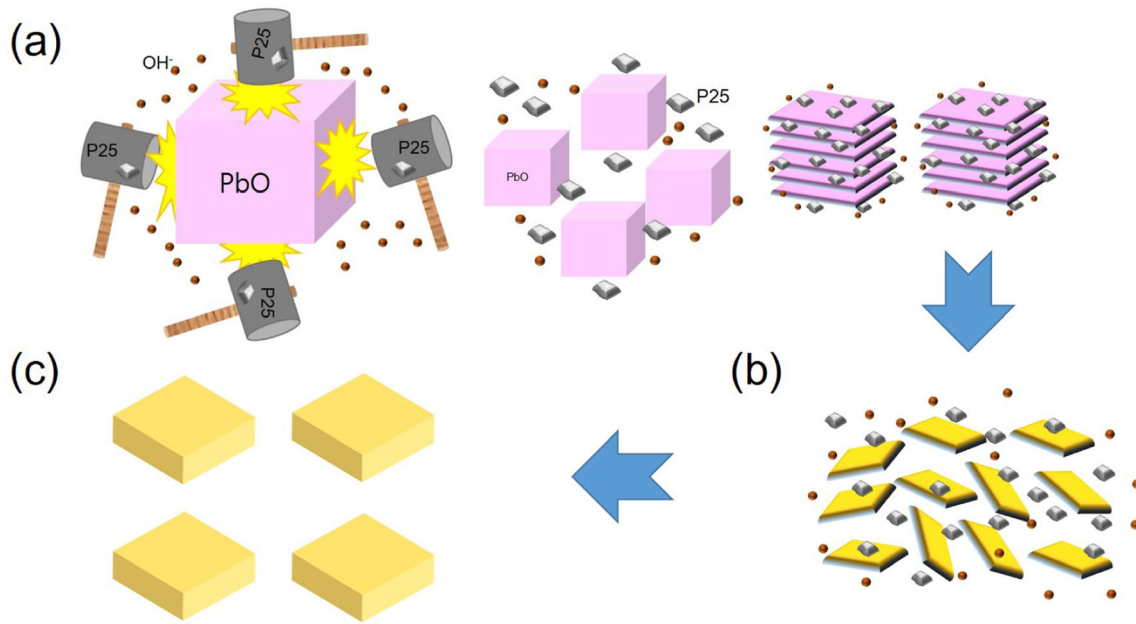
Fig. 6 Schematic image showing the growth process of the PbTiO₃ nanoplates. **a** The larger PbO crystals were crushed into smaller crystals by the P25-TiO₂ particles and exfoliated into layered structures; **b** dispersive PbTi$_x$O$_y$ thinner plates mixed with the unreacted P25-TiO₂ particles; **c** the final PbTiO₃ nanoplates

inset image shows an AFM topographic image of a single PbTiO₃ nanoplate. The d_{33} value of the PbTiO₃ nanoplates is estimated to be approximately 165 pm/V based on the curve. Compared with the d_{33} values of PbTiO₃ single crystals (117 or 143 pC N^{-1}) summarized by Yan et al. [40], this value is greatly enhanced due to the preferable growth of the {001} planes (<001>orientation), which could be used to produce <001>-textured Pb-based piezoelectric ceramics [11, 12].

4 Conclusions

To conclude, PbTiO₃ nanoplates with an aspect ratio of approximately 5 were successfully synthesized by a hydrothermal method. To evaluate the effect of different growth parameters on the growth of the nanoplates, a series of experiments related to the concentration of the mineralizer (KOH), Pb^{2+}/Ti^{4+} ratio and heating time, etc. were performed. The best growth conditions were set as 200 °C/10 h, Pb^{2+}/Ti^{4+} = 1.25 (M$_{P25}$ = 5 mmol and M$_{Pb(NO3)2}$ = 6.25 mmol), M$_{KOH}$ = 8 mol/L (in 30 ml of DI water) with P25-TiO₂ and Pb(NO₃)₂ as the source materials. In addition, a modified growth process of the PbTiO₃ nanoplates was proposed by studying the results at different synthesis durations. Furthermore, d_{33} versus the applied voltage showed a good hysteresis curve with a maximum d_{33} value of ∼ 165 pm/V, indicating good ferroelectric behaviors of the as-synthesized PbTiO₃ nanoplates.
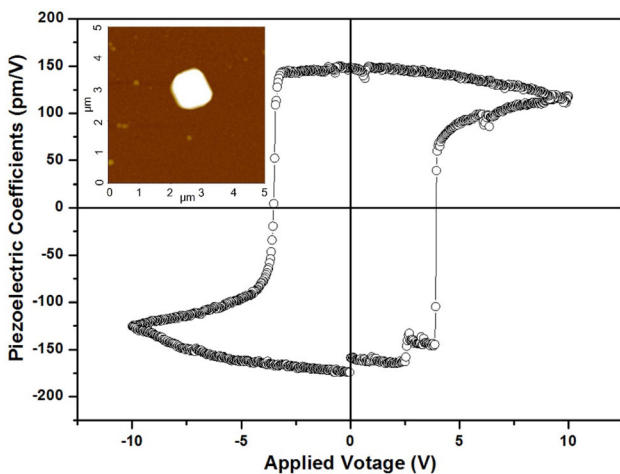

Fig. 7 d_{33} versus E curves of the PbTiO₃ nanoplates; the inset image shows an AFM topographic image of a single PbTiO₃ nanoplate

Acknowledgements

Data Availability

All data generated or analyzed during this study are included in this published article [and its supplementary material file].

Compliance with ethical standards

Conflict of interest The authors declare that they have no conflict of interest.

Supplementary Information: The online version contains supplementary material available at http s://doi.org/10.1007/s10854-021-05325-7.

References

1. Z.R. Li, X. Yao, Dielectric, pyroelectric and piezoelectric properties of $(1-x)Pb(Ni_{1/3}Nb_{2/3})O_3-xPbTiO_3$ system. J. Mater. Sci. Lett. **20**, 273–275 (2001)

2. X.P. Wang, J.G. Wu, D.Q. Xiao, J.G. Zhu, X.J. Cheng, T. Zheng, B.Y. Zhang, X.J. Lou, X.J. Wang, Giant piezoelectricity in potassium−sodium niobate lead-free ceramics. J. Am. Chem. Soc. **136**, 2905–2910 (2014)

3. K.-T. Lee, D.-H. Kim, S.-H. Cho, J.-S. Kim, J.-H. Ryu, C.-W. Ahn, T.-H. Lee, G.-H. Kim, S. Nahm, Pseudocubic-based polymorphic phase boundary structures and their effect on the piezoelectric properties of (Li, Na, K)(Nb, Sb)O_3-SrZrO$_3$ lead-free ceramics. J. Alloys Compd. **784**, 1334–1343 (2019)

4. X.H. Ma, Z.L. Zhang, T.W. Xu, S.L. Zhang, Correlation between cubic-based polymorphic phase boundary structures and the piezoelectric properties of $0.96(Na_{0.5}K_{0.5})(Nb_{1-x}Sb_x)$-$0.04BaTiO_3$ ceramics. J. Asian Ceram. Soc. **4**, 1127–1134 (2020)

5. K. Takahashi, M. Nishida, H. Hase, Effect of Y and Mn doping in Pb(T, Zr)O_3 piezoelectric ceramics on the resonant frequency and capacitance changes and aging by thermal shock tests. Jpn. J. Appl. Phys. **37**, 5285–5287 (1998)

6. H.Y. Park, C.H. Nam, I.T. Seo, J.H. Choi, S. Nahm, H.G. Lee, K.J. Kim, S.M. Jeong, Effect of MnO$_2$ on the piezoelectric properties of the $0.75Pb(Zr_{0.47}Ti_{0.53})O_3-0.25Pb(Zn_{1/3}Nb_{2/3})O_3$ ceramics. J. Am. Ceram. Soc. **93**, 2537–2540 (2010)

7. X.L. Huang, Y.X. Tang, F.F. Wang, X.Y. Zhao, Z.H. Duan, T. Wang, Q.X. Du, J.S. Wang, X.T. Zhou, W.Z. Shi, Piezoelectric and pyroelectric properties of Mn-doped $0.36Pb(In_{1/2}Nb_{1/2})O_3-0.36Pb(Mg_{1/3}Nb_{2/3})O_3-0.28PbTiO_3$ ceramics. J. Mater. Sci. Mater. Electron. **31**, 14426–14433 (2020)

8. B.J. Tao, W.F. Wang, H.Y. Liu, T.X. Du, H.T. Wu, C.F. Xing, D.Z. Wang, Y.P. Zhang, Low-temperature sintering LiF-doped $Li_4Mg_3[Ti_{0.6}(Mg_{1/3}Nb_{2/3})_{0.4}]_2O_9$ microwave dielectric ceramics for LTCC applications. Ceram. Int. **47**, 2584–2590 (2021)

9. E.M. Sabolsky, A.R. James, S. Kwon, S. Trolier-Mckinstry, G.L. Messing, Piezoelectric properties of <001> textured $Pb(Mg_{1/3}Nb_{2/3})O_3$-PbTiO$_3$ ceramics. App. Phy. Lett. **78**, 2551–2553 (2001)

10. Y. Saito, H. Takao, T. Tani, T. Nonoyama, K. Takatori, T. Homma, T. Nagaya, M. Nakamura, Lead-free piezoceramics. Nature **432**, 84–87 (2004)

11. Y.K. Yan, K.H. Cho, D. Maurya, A. Kumar, S. Kalinin, A. Khachaturyan, S. Priya, Giant energy density in [001]-textured $Pb(Mg_{1/3}Nb_{2/3})O_3$-PbZrO$_3$-PbTiO$_3$ piezoelectric ceramics. Appl. Phys. Lett. **102**, 042903 (2013)

12. S.T. Kwon, E.M. Sabolsky, G.L. Messing, S. Trolier-McKinstry, High Strain, <001> textured $0.675Pb(Mg_{1/3}Nb_{2/3})O_3-0.325PbTiO_3$ ceramics: Templated grain growth and piezoelectric properties. J. Am. Ceram. Soc. **88**, 312–317 (2005)

13. J.A. Horn, S.C. Zhang, U. Selvaraj, G.L. Messing, S. Trolier-McKinstry, Templated grain growth of textured bismuth titanate. J. Am. Ceram. Soc. **82**, 921–926 (1999)

14. G.L. Messing, S.T. McKinstry, E.M. Sabolsky, C. Duran, S. Kwon, B. Brahmaroutu, P. Park, H. Yilmaz, P.W. Rehrig, K.B. Eitel, E. Suvaci, M. Seabaugh, K.S. Oh, Templated grain growth of textured piezoelectric ceramics. Crit. Rev. Solid State Mater. Sci. **29**, 45–96 (2004)

15. Y.K. Yan, Y.U. Wang, S. Priya, Electromechanical behavior of [001]-textured $Pb(Mg_{1/3}Nb_{2/3})O_3$-PbTiO$_3$ ceramics. Appl. Phys. Lett. **100**, 192905 (2012)

16. K.H. Brosnan, S.F. Poterala, R.J. Meyer, S. Misture, G.L. Messing, Templated grain growth of <001> textured PMN-28PT using SrTiO$_3$ templates. J. Am. Ceram. Soc. **92**, S133–S139 (2009)

17. D. P. Maurya, Y. Zhou, Y. K. Yan, S. Priya, Synthesis mechanism of grain-oriented lead-free piezoelectric $Na_{0.5}Bi_{0.5}TiO_3$–BaTiO$_3$ ceramics with giant piezoelectric response. J. Mater. Chem. C 1, 2102–2111 (2013)

18. A. Berksoy-Yavuz, U. Savaci, S. Turan, S. Alkoy, E. Mensur-Alkoy, Structural features and energy harvester device applications of textured 0.675 PMN–0.325 PT piezoceramics, J. Mater. Sci. Mater. Electron. 31, 9650–9659 (2020)

19. D. Liu, Y.K. Yan, H.P. Zhou, Synthesis of micron-scale platelet BaTiO$_3$. J. Am. Ceram. Soc. **90**, 1323–1326 (2007)

20. M.E. Ebrahimi, M. Allahverdi, A. Safari, Synthesis of high aspect ratio platelet SrTiO$_3$. J. Am. Ceram. Soc. **88**, 2129–2132 (2005)

21. C.H. Hong, H.P. Kim, B.Y. Choi, H.S. Han, J.S. Son, C.W. Ahn, W. Jo, Lead-free piezoceramics-Where to move on? J. Materiomics **2**, 1–24 (2016)

22. T.G. Lee, H.J. Lee, D.H. Kim, H.B. Xu, S.J. Park, J.S. Park, S. Nahm, C.Y. Kang, S.J. Yoon, Relation between structure and piezoelectric properties of (1-x-y)PbZrO$_3$-xPbTiO$_3$-yPb(Ni$_{1/3}$Nb$_{2/3}$)O$_3$ ceramics near triple point composition. J. Eur. Ceram. Soc. **36**, 4049–4057 (2016)

23. F. Li, D.B. Lin, Z.B. Chen, Z.X. Cheng, J.L. Wang, C.C. Li, Z. Xu, Q.W. Huang, X.Z. Liao, L.Q. Chen, T.R. Shrout, S.J. Zhang, Ultrahigh piezoelectricity in ferroelectric ceramics by design. Nature Mater. **17**, 349–354 (2018)

24. E.J. Kim, T.G. Lee, D.S. Kim, S.W. Kim, Y.J. Yee, S.H. Han, H.W. Kang, S. Nahm, Textured Pb(Zr, Ti)O$_3$-Pb[(Zn, Ni)$_{1/3}$Nb$_{2/3}$]O$_3$ multilayer ceramics and their application to piezoelectric actuators. Appl. Mater. Today **20**, 100695 (2020)

25. C.Y. Chao, Z.H. Ren, Y.H. Zhu, Z. Xiao, Z.Y. Liu, G. Xu, J.Q. Mai, X. Li, G. Shen, G.R. Han, Self-templated synthesis of single-crystal and single-domain ferroelectric nanoplates. Angew. Chem. Int. Ed. **51**, 9283–9287 (2012)

26. S.Q. Deng, G. Xu, H.W. Bai, L.L. Li, S. Jiang, G. Shen, G.R. Han, Hydrothermal synthesis of single-crystalline perovskite PbTiO$_3$ nanosheets with dominant (001) facets. Inorg. Chem. **53**, 10937–10943 (2014)

27. B. Ohtani, O.O. Prieto-Mahaney, D. Li, R. Abe, What is Degussa (Evonik) P25? Crystalline composition analysis, reconstruction from isolated pure particles and photocatalytic activity test. J. Photochem. Photobiol. A: Chem. **216**, 179–182 (2010)

28. X.H. Ma, H.Y. Li, S.H. Kweon, S.Y. Jeong, J.H. Lee, S. Nahm, Highly sensitive and selective PbTiO$_3$ gas sensors with negligible humidity interference in ambient atmosphere. ACS Appl. Mater. Interfaces **11**, 5240–5246 (2019)

29. J.B. Gao, H.Y. Shi, H.N. Dong, R. Zhang, D.L. Chen, Factors influencing formation of highly dispersed BaTiO$_3$ nanospheres with uniform sizes in static hydrothermal synthesis. J. Nanopart. Res. **17**, 286 (2015)

30. X.H. Ma, S.H. Kweon, S. Nahm, C.Y. Kang, S.J. Yoon, Y.S. Kim, W.S. Yoon, Microstructural and Microwave Dielectric Properties of Bi$_{12}$GeO$_{20}$ and Bi$_2$O$_3$-Deficient Bi$_{12}$GeO$_{20}$ Ceramics. J. Am. Ceram. Soc. **99**, 2361–2367 (2016)

31. L. Li, L.Z. Liang, H. Wu, X.H. Zhu, One-dimensional perovskite manganite oxide nanostructures: Recent developments in synthesis, characterization, transport properties, and applications. Nanoscale Res. Lett. **11**, 121 (2016)

32. Y.M. Rangel-Hernandez, J.C. Rendón-Angeles, Z. Matamoros-Veloza, M.I. Pech-Canul, S. Diaz-de la Torre, K. Yanagisawa, One-step synthesis of fine SrTiO$_3$ particles using SrSO$_4$ ore under alkaline hydrothermal conditions. Chem. Eng. J. **155**, 483–492 (2009)

33. Y. Wang, X.C. Yan, J. Chen, J.X. Deng, R.B. Yu, X.R. Xing, Shape controllable synthesis of NdFeO$_3$ micro single crystals by a hydrothermal rout. CrystEngComm **16**, 858–862 (2014)

34. G. Philippot, C. Elissalde, M. Maglione, C. Aymonier, Supercritical fluid technology: A reliable process for high quality BaTiO$_3$ based nanomaterials. Adv. Powder Technol. **25**, 1415–1429 (2014)

35. Y.K. Tak, S. Pal, P.K. Naoghare, S. Rangasamy, J.M. Song, Shape-Dependent Skin Penetration of Silver Nanoparticles: Does It Really Matter? Sci. Rep. **5**, 16908 (2015)

36. Z.M. Cui, H. Yang, B. Wang, R.S. Li, X.X. Wang, Effect of Experimental Parameters on the Hydrothermal Synthesis of Bi$_2$WO$_6$ Nanostructures. Nanoscale Res. Lett. **11**, 190 (2016)

37. J.Q. Zhang, K.K. Huang, L. Yuan, S.H. Feng, Mineralizer effect on facet-controllable hydrothermal crystallization of perovskite structure YbFeO$_3$ crystals. CrystEngComm **20**, 470–476 (2018)

38. M.M. Lencka, R.E. Riman, Synthesis of lead titanate: Thermodynamic modeling and experimental verification. J. Am. Ceram. Soc. **76**, 2649–2659 (1993)

39. H.B. Xu, Y.J. Ko, T.G. Lee, S.J. Park, M.S. Noh, B.Y. Kim, J.S. Kim, S. Nahm, Structural and piezoelectric properties of (Na$_{1-x}$K$_x$)NbO$_3$ platelets and their application for piezoelectric nanogenerator. J. Am. Ceram. Soc. **99**, 3476–3484 (2016)

40. Y.K. Yan, J.E. Zhou, D. Maurya, Y.U. Wang, S.S. Priya, Giant piezoelectric voltage coefficient in grain-oriented modified PbTiO$_3$ material. Nat. Commun. **7**, 13089 (2016)